The role of conceptual models in climate research

Henk A. Dijkstra *

Institute for Marine and Atmospheric Research Utrecht, Department of Physics, Utrecht University, Utrecht, The Netherlands
Center for Complex Systems Studies, Department of Physics, Utrecht University, Utrecht, The Netherlands

ARTICLE INFO

ABSTRACT

Climate variability occurs on a multitude of temporal and spatial scales and the associated phenomena are studied using observations and a hierarchy of climate models. The aim of this paper is to describe the role that relatively simple models, usually referred to as conceptual climate models, have in the understanding of climate variability phenomena. To illustrate the importance of these conceptual models, we focus here exclusively on the tipping of the Atlantic Meridional Overturning Circulation (AMOC) under a changing surface freshwater forcing. In this case, results from the full hierarchy of models are available. Conceptual climate models and their mathematical analysis have generated basic physical concepts of AMOC tipping. In addition, these results have served as an important interpretation framework for more detailed models up to state-of-the-art global climate models.

1. Introduction

Over recent decades, a new field of science has developed which could be labeled 'Mathematics of Climate'. Here, climate scientists are collaborating with mathematicians to gain more detailed insights into phenomena of climate variability and climate change. In 2013, the first book [1] in this field appeared, published by the Society of Industrial and Applied Mathematics (SIAM) wherein a mosaic of mathematical topics (e.g. Dynamical Systems) and climate dynamics topics (e.g. El Niño/Southern Oscillation) is presented. Mathematics of Climate is also part of the more broader theme 'Mathematics of Planet Earth' where not only climate is a central topic, but also other Earth System components, such as Earth's interior. Researchers in this broader area interact on many events, such as during the SIAM Conference on Mathematics of Planet Earth, which is organized biannually.

It is important that mathematicians are involved in climate research because a fundamental shift has taken place over the last decades. The old paradigm of linear and gradual change in planetary-scale behavior due to slowly varying forcing is being replaced by a new paradigm of nonlinear and possibly abrupt multi-scale climate changes. This can be inferred from the succession of reports of the Intergovernmental Panel on Climate Change, in which concepts of transitions, responsible for abrupt change and extreme events, have become more prominent over the years [2,3]. A proper analysis of such phenomena requires more sophisticated mathematical techniques than those commonly used (e.g. multivariate linear statistics) in the climate research community.

Although there was already much previous work on transition behavior in several climate subsystems [4–6], it was the paper [7] that

put the concept of 'climate tipping' on the forefront of attention to the broader research community. There is now a reasonable consensus on which climate subsystems should be labeled as tipping elements, i.e. which can undergo tipping behavior [8]. Also estimates have been provided on the degree of global warming for which the tipping point in each of these subsystems can be crossed [8]. The concept of tipping is no longer concerned only with the occurrence of bifurcations tipping, because transitions can also be noise induced or rate induced [9]. However, the occurrence of bifurcation behavior is still crucial to both other forms of tipping as it will create the multiple attractor structure required.

Since experimental options for Earth's climate system are limited, climate models are the key to understanding the behavior of the past and present-day climate system, as well as to making projections of future climate change. It is up to climate researchers to choose a climate model which is thought to be fit for purpose to answer the leading questions on their mind. A whole hierarchy is available, from models with only a few unknowns to models with billions of unknowns [10]. The models on the low end of this model hierarchy are often referred to as conceptual climate models.

This paper is written with a researcher in mind who is interested in studying climate phenomena using conceptual models. In Section 2, we start with an overview of the climate model hierarchy to give an idea what type of models are available in climate research and to put the conceptual models into a broader context. Then, in Section 3, we focus on a much studied climate subsystem, the Atlantic Meridional Overturning Circulation (AMOC), and show how conceptual models have
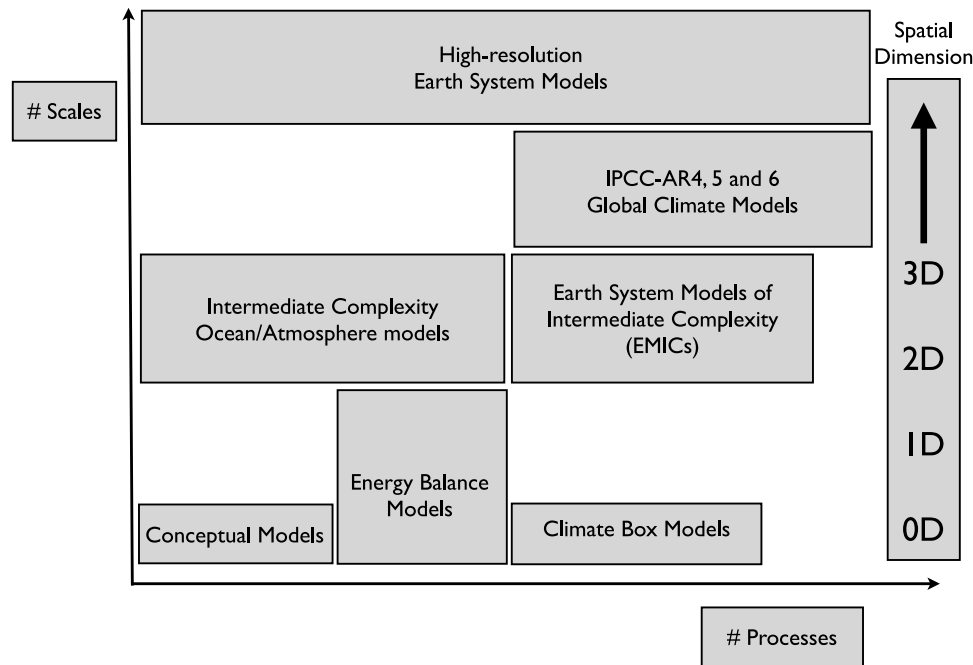
Fig. 1. 'Classification' of climate models according to the two model traits: number of processes and number of scales. Here 0D (zero dimensional), 1D (one dimensional), 2D (two dimensional) and 3D (three dimensional) indicate the spatial dimension of the model.
Source: Modified from [10].

contributed to the understanding of tipping behavior of the AMOC. In the last section, a summary and discussion is provided, also putting the AMOC results in the broader context of the role of conceptual models in climate research.

2. The climate modeling hierarchy

In climate research, a wide range of models is in use from 'very simple' conceptual climate models (abbreviated in this paper as CCMs) to 'very complicated' models, usually referred to as state-of-the-art Global Climate Models (GCMs) or Earth System Models (ESMs). To obtain a rough overview of these different models, the model traits 'scales' and 'processes' are sometimes used [10]. Here the trait 'scales' refers to both spatial and temporal scales as there exists a relation between both: on smaller spatial scales usually faster processes take place. 'Processes' refers to either physical, chemical or biological processes taking place in the different climate compartments (atmosphere, ocean, cryosphere, biosphere, lithosphere). Both traits affect the dimension of the state vector of the resulting dynamical system in a different way. For example in a 3D model, with a grid of N, M, and L points in x, y and z direction, respectively, and K unknowns per grid point the state vector dimension $d = N \times M \times L \times K$. Doubling the horizontal resolution would result in $d = 4N \times M \times L \times K$ while by adding a set of new equations for additional unknowns (representing new processes), d would just linearly increase (with K).

The CCMs are those models with a limited number of processes and scales (Fig. 1). In these models only very specific interactions in the climate system are described and only a limited representation of spatial structure is captured. In a large class of such models, the ocean or atmosphere is represented as a set of boxes which exchange properties, such as water, moisture and heat. Examples of such models will be given in Section 3 below. The number of processes between the boxes can be extended, for example by including sea-ice, land-ice processes or biogeochemical processes. In this way, one ends up in the right bottom part of the diagram in Fig. 1 since the number of scales is still relatively small. An example is the LOSCAR model [11], used to study biogeochemical cycles in the geological past. An increase

in the number of boxes may increase the number of (spatial) scales represented but the model will still consist of a system of ordinary differential equations (ODEs).

Limiting the number of processes, scales can be added by discretization of the governing partial differential equations (PDEs) spatially up to three dimensions. A higher spatial resolution and inclusion of more processes will give models located in the right upper part of the diagram. In a GCM, the atmosphere, ocean, ice and land components are divided into control volumes. Over such a control volume the budgets of momentum, mass and for example heat are then evaluated. For example, momentum budgets basically follow from Navier–Stokes equations formulated for air and water. With an increasing number of control volumes, however, the time development of an increasing number of quantities has to be calculated. The same holds for the number of processes included in a GCM: more processes simply means more calculations. Doubling the horizontal resolution will typically increase computational costs by about a factor 10 as also the time step has to halved. Also the longer time period over which we want to compute the development of each quantity the longer it takes to do the calculation on a computer. A climate model code genealogy was recently presented in [12] and an overview of state-of-the-art models used in the Intergovernmental Panel of Climate Change latest report can be found in Chapter 1 of [13].

Compared to GCMs, the ocean and atmosphere models in Earth System Models of Intermediate Complexity (EMICs) are strongly reduced in the number of scales [14]. For example, the atmospheric model may consist of a shallow-water model and the ocean component may be a zonally averaged model. The advantage of EMICs is therefore that they are computationally less demanding than GCMs and hence many more long-time scale processes, such as land-ice and carbon cycle processes can be included. Each of the individual component models of EMICs may also be used to study the interaction of a limited number of processes. Modern EMICs are Climber-X [15] and iLOVECLIM [16]. In time, the GCMs of today will be the EMICs of the future and the state-of-the-art GCMs will shift upwards to high resolution versions of ESMs, possibly with new processes added (Fig. 1a).

There is no 'unified' climate model with which one is able to tackle any scientific question on the climate system and there will never be.
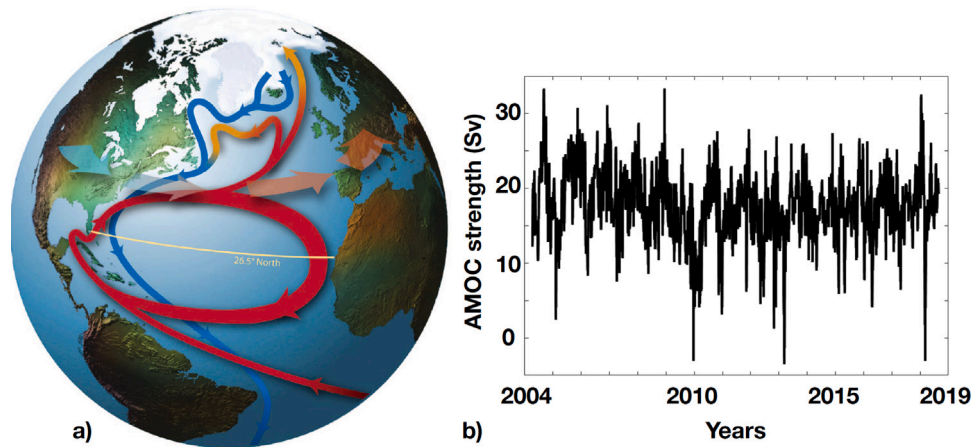
Fig. 2. (a) Sketch of the Atlantic Ocean circulation ([[17], figure reprinted with permission from the American Meteorological Society) with warm water flowing north in the upper ocean (red), which releases heat to the atmosphere, sinks, and returns as a deep cold flow (blue). The latitude of the 26°N RAPID-MOCHA array is indicated (yellow). (b) Observed strength of the AMOC (in Sverdrup Sv, where 1 Sv = 10^6 m^3 s^{-1}) from the RAPID-MOCHA array at about 1000 m depth.

The choice of a particular model is motivated by the specific question asked. For example, if one wants to study the behavior of a globally averaged quantity (e.g. the global mean surface temperature) then a CCM may be fit for purpose. However, if one wants to study spatial patterns, e.g. that associated with El Niño/Southern Oscillation (ENSO), then a spatially extended model (formulated by PDEs) is required. Often, a specific phenomenon is studied using a hierarchy of models, where the models lower in the hierarchy (e.g., CCMs) are used for studying mechanisms, while those higher up in the hierarchy (e.g. GCMs) are used to compare to observations and for making projections (e.g., of climate change). Model choice is also based on practical limitations such as the computational platform which is available.

3. Tipping of the AMOC

The full hierarchy of models, as described in the previous section, has been applied to study the behavior of the AMOC under changing forcing conditions. The AMOC is one of the main tipping elements identified in [8], in addition to the Subpolar Gyre, the Polar (Greenland and Antarctic) Ice Sheets, the Amazon Forest, the Arctic Sea Ice and the Boreal Permafrost. Based on expert knowledge, the AMOC is thought to tip when the global mean surface temperature increases by about 4 °C with respect to pre-industrial [8].

3.1. AMOC observations

A sketch of the Atlantic Ocean circulation is provided [18] in Fig. 2a and the AMOC is the zonally-averaged volume transport associated with this circulation. The surface component of the AMOC is formed by relatively warm and salty waters that cool on their path northwards. In the sub-polar regions, deepwater formation occurs leading to southward transport of cooler and fresher water at mid-depth [19]. In this way, the AMOC carries as much as 90% of all the heat transported polewards by the subtropical Atlantic Ocean [20].

While the existence of the AMOC can already be deduced from measurements of salinity, only few direct measurements of the AMOC were available before the year 2000 [21]. At the moment, continuous section measurements are available at 26°N (RAPID-MOCHA) and along the northern (OSNAP), and the southern (SAMBA) boundary of the Atlantic [22]. The strength of the AMOC is the maximum value of the vertical integral (from the surface downward) of the zonally integrated meridional volume transport. At 26°N this maximum is located at a depth of about 1,100 m. From the RAPID-MOCHA measurements (Fig. 2b), the mean AMOC strength is about 17 Sv [22]. It has decreased by a few Sv from 2004 to 2012 and thereafter it has recovered [23].

There is also substantial variability on interannual (and smaller) time scales.

Longer time scale variability of the AMOC strength was estimated by using sea surface temperature (SST) patterns in the subpolar northern Atlantic Ocean and in the Gulf Stream region [24]. This SST-based 'fingerprint' indicates that the AMOC weakened by 3 ± 1 Sv since about 1950 and, using proxy records, that the AMOC is currently in its weakest state in over a millennium [25]. However, in a recent analysis of the available array and hydrographic measurements [26] no long-term AMOC decline has been found over the period 1982–2016. Hence, SST-based measures may not give a complete view of the AMOC because they do not adequately capture changes in the deep circulation [26].

Although no AMOC collapses have been observed in historical measurements, there is much evidence from proxy data that such transitions have occurred in the geological past [27]. In particular, transitions between strong and weak AMOC states were likely involved in millennial time scale changes in Northern Hemisphere temperatures during the last glacial period [28], the so-called Dansgaard–Oeschger events [29]. Here, temperature anomalies reconstructed from high-resolution isotope records (e.g. from ice cores on Greenland) are linked to changes in the meridional heat transport due to the AMOC changes [30].

3.2. Deterministic conceptual models: North Atlantic

Density differences in the ocean are essential for the existence of the AMOC mean state and AMOC variability. Temperature T and salinity S affect density in an opposite way, and a linear equation of state

$$\rho = \rho_0(1 - \alpha_T(T - T_0) + \alpha_S(S - S_0)), \tag{1}$$

is often an adequate approximation of the more detailed relation. Here, the subscript '0' refers to reference values and α_T and α_S are the positive (and constant) thermal expansion and haline contraction coefficients, respectively. Two feedbacks have been identified to affect the AMOC strength and its variability: an advective feedback and a convective feedback. In the two subsections below, conceptual models of these feedbacks are presented.

3.2.1. Advective feedback

In a seminal paper [32], it was realized that there is a nonlinear coupling between the AMOC and the density field: the AMOC advects density anomalies but the density field affects the AMOC. The consequences of this nonlinear coupling of the temperature, salinity and AMOC were studied in its simplest form using a two-box model. A sketch of a variant of this model [31] is shown in Fig. 3a.
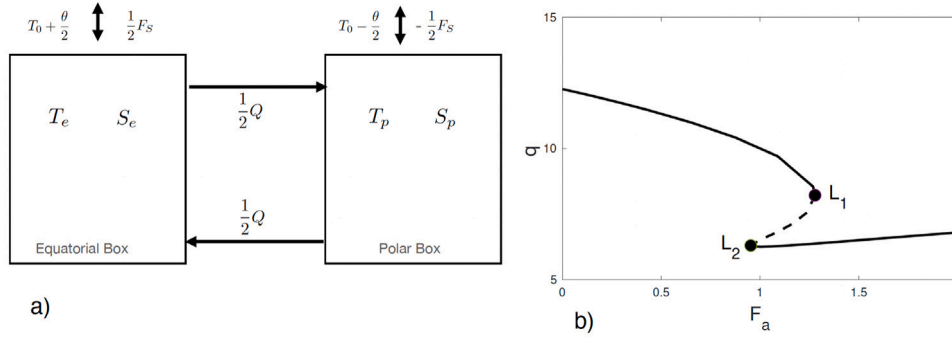
Fig. 3. (a) A Stommel-type two-box model of the Atlantic MOC as formulated by [31]. (b) Bifurcation diagram of the model (18) for $\alpha = 360$ and $\mu = 6.25$, showing the dimensionless AMOC strength $q = 1 + \mu(x - y)^2$ versus F_a.

A polar box (with temperature T_p and salinity S_p) and an equatorial box (with temperature T_e and salinity S_e) having the same volume V_0 are connected by an overturning flow and exchange heat and fresh water with the atmosphere. The heat and salt balances are [31]

$$\frac{dT_e}{dt} = -\frac{1}{t_r}(T_e - (T_0 + \frac{\theta}{2})) - \frac{1}{2}Q(\Delta\rho)(T_e - T_p), \tag{2a}$$

$$\frac{dT_p}{dt} = -\frac{1}{t_r}(T_p - (T_0 - \frac{\theta}{2})) - \frac{1}{2}Q(\Delta\rho)(T_p - T_e), \tag{2b}$$

$$\frac{dS_e}{dt} = \frac{F_S}{2H}S_0 - \frac{1}{2}Q(\Delta\rho)(S_e - S_p), \tag{2c}$$

$$\frac{dS_p}{dt} = -\frac{F_S}{2H}S_0 - \frac{1}{2}Q(\Delta\rho)(S_p - S_e), \tag{2d}$$

where F_S is the freshwater flux forcing, H the ocean depth, t_r is the surface temperature restoring time scale and θ is the equator-to-pole atmospheric temperature difference. Note that when $F_S > 0$ ($F_S < 0$), more (less) fresh water will enter the polar box decreasing (increasing) the salinity of that box In [31], the transport function Q is chosen as

$$Q(\Delta\rho) = \frac{1}{t_d} + \frac{q_0}{V_0}(\frac{\Delta\rho}{\rho_0})^2, \tag{3}$$

where q_0 is a transport coefficient, t_d a diffusion time and $\Delta\rho = \rho_p - \rho_e$.

To obtain dimensionless equations, $\Delta T = T_e - T_p$ and $\Delta S = S_e - S_p$ are introduced, non-dimensional new variables x and y are defined by $\Delta T = x \theta$, $\Delta S = y \alpha_T \theta / \alpha_S$ and time is scaled by t_d. This leads to the equations

$$\frac{dx}{dt} = -\alpha(x - 1) - x(1 + \mu(x - y)^2), \tag{4a}$$

$$\frac{dy}{dt} = F_a - y(1 + \mu(x - y)^2), \tag{4b}$$

with parameters

$$\alpha = t_d/t_r \; ; \; \mu = \frac{q_0 t_d(\alpha_T \theta)^2}{V_0} \; ; \; F_a = \frac{\alpha_S S_0 t_d}{\alpha_T \theta H}F_S. \tag{5}$$

Here F_a is the dimensionless freshwater forcing strength and typical values of the non-dimensional parameters, as motivated in [33], are $\alpha = 360$, $F = 1.1$ and $\mu = 6.25$.

The bifurcation diagram of (4), plotting the dimensionless AMOC strength $q = 1 + \mu(x - y)^2$ versus F_a, is shown in Fig. 3b. Here the dashed curves indicate unstable steady states and the drawn curves stable ones. The interval of multiple states is bounded by the two saddle–node bifurcations L_1 and L_2 and the associated interval in F_a is the multiple equilibrium regime. In this conceptual view, the present-day AMOC state is sensitive to changes to its North Atlantic surface freshwater flux. This is due to the so-called salt-advection feedback: freshwater anomalies in the North Atlantic will decrease the strength of the AMOC, thereby decreasing the northward salt transport and hence amplifying the original freshwater anomaly [34].

There are many variants of these box models, each designed for addressing a specific problem, which are motivated by either observations

or by results from GCMs and/or EMICs. A more physically consistent transport relation for Q is used in [35], additional deep boxes are added in [36] to explain oscillatory behavior of the AMOC, and a different box configuration (with two polar boxes coupled to one equatorial box) is used in [37] to study the effects on different Labrador and Irminger Sea transports on the AMOC. The latter study was motivated by recent observational results [38] from the OSNAP array in the northern North Atlantic.

3.2.2. Convective feedback

It was also realized a long time ago by Welander [39] that convective processes, arising from static instability (i.e. a layer of heavy water above light water), could affect the AMOC. A slightly modified version of the model in [39] was presented in [40]. Consider (Fig. 4a) a surface box with time-varying temperature T and salinity S due to a surface heat flux $F_T = \gamma(T_A - T)$ and surface freshwater flux F_S. Convective exchange with mixing coefficient κ occurs if the surface water becomes denser than the water in the bottom box, which has constant (reference) temperature T_0 and salinity S_0.

The equations for the evolution of the temperature T and S are

$$\frac{dT}{dt} = \gamma(T_A - T) - \kappa(T - T_0), \tag{6a}$$

$$\frac{dS}{dt} = -\frac{F_S S_0}{H} - \kappa(S - S_0), \tag{6b}$$

where H is a depth scale. The mixing coefficient κ is given by

$$\kappa = \begin{cases} \kappa_1, \rho - \rho_0 \le \Delta\rho, \\ \kappa_2, \rho - \rho_0 > \Delta\rho, \end{cases} \tag{7}$$

where $\kappa_2 \gg \kappa_2$ and $\Delta\rho$ is a small negative number so strong mixing occurs when heavy water overlies lighter water.

With the introduction of $x = (T - T_0)/(T_A - T_0)$, $S = \alpha_S(S - S_0)/(\alpha_T(T_A - T_0))$, scaling time with γ, and using (1), the dimensionless equations become

$$\frac{dx}{dt} = 1 - x - \nu x, \tag{8a}$$

$$\frac{dy}{dt} = F_c - \nu y, \tag{8b}$$

where

$$\nu = \begin{cases} \nu_1 = \frac{\kappa_1}{\gamma}, y - x \le r, \\ \nu_2 = \frac{\kappa_2}{\gamma}, y - x > r, \end{cases} \tag{9}$$

with parameters

$$r = \frac{\Delta\rho}{\rho_0\alpha_T(T_A - T_0)} \; ; \; F_c = -\frac{\alpha_S F_S}{\alpha_T H\gamma(T_A - T_0)}. \tag{10}$$

A typical bifurcation diagram for the case that the function ν is smoothed by an approximation of the Heaviside function $\mathcal{H}$, i.e.

$$\nu = \nu_1 + (\nu_2 - \nu_1)\mathcal{H}(y - x - \epsilon), \tag{11a}$$
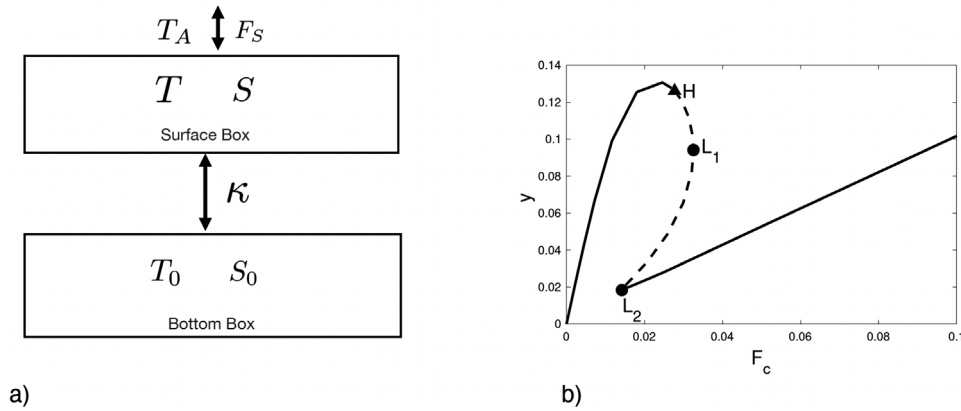
Fig. 4. (a) Sketch of a Welander-type box model set-up to illustrate the convective feedback [39,40]. (b) Bifurcation diagram of the model (8b) for $r = -0.6$, $v_1 = 0.1$, $v_2 = 1.0$, $\epsilon = 0.1$.
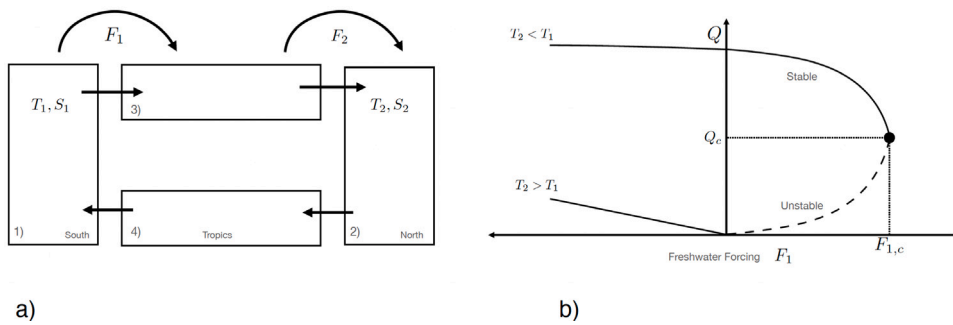
Fig. 5. (a) Box model used in [47] with the freshwater transports indicated by F_1 and F_2, respectively. (b) The different flow regimes in the box model depending on the prescribed temperature difference $T_2 - T_1$.

$$\mathcal{H}(z) = \frac{1}{2}(1 + \tanh \frac{z}{\epsilon}), \tag{11b}$$

is shown in Fig. 4b. Again two saddle–node bifurcations are found, in addition to a Hopf bifurcation, giving a region of multiple stable states. The underlying feedback is a convective one: when a salt perturbation is added to the upper layer of a non-convecting state (with a fresher and colder upper layer than the bottom layer), a transition to a convective state can occur. This mixes warmer and saltier water from the bottom box upwards. The heat in the surface layer is quickly lost to the atmosphere, but the surface salinity is increased and hence convection is maintained. The detailed bifurcation diagrams, both for the non-smooth case and the smoothed case, are worked out in [41].

As the convective feedback influences the vertical density distribution, it also influences the AMOC due to horizontal density differences. In [42,43], a Stommel model is connected to a Welander-type model leading to quite complicated dynamics as both advective and convective feedbacks can interact. With this box model, it was aimed to explain millennial time scale oscillations, so-called flushes or deep-decoupling oscillations, seen in ocean-only GCMs [44] and EMICs [45].

3.3. Deterministic conceptual models: inter-hemispheric Atlantic

The models in the previous section only considered the AMOC in the North Atlantic, while the AMOC clearly involves both North and South Atlantic. Independently of the Stommel model, an inter-hemispheric model of the AMOC was suggested in [46]. The model consists of three boxes, two polar and one equatorial, and the AMOC is assumed to be driven by the pole-to-pole density difference. Whereas the temperature in the boxes is prescribed, the salinities are varying due to freshwater fluxes.

The model in [46] was extended by [47] to include a deep equatorial box and the steady equation for the salinity in the (active) box 1 is

$$S_0 F_1 + Q(S_2 - S_1) = 0. \tag{12}$$

where F_1 is the freshwater transport as indicated in Fig. 5a, S_0 is a reference salinity and the AMOC strength is given by

$$Q = k \left(\alpha_S (S_2 - S_1) - \alpha_T (T_2 - T_1) \right), \tag{13}$$

where k is transport coefficient. When $F_1 > 0$, freshwater is transported out of the southern box, increasing its salinity and hence weakening the AMOC strength and vice versa.

When (12) is combined with (13), the steady-state AMOC transport is a solution of the quadratic equation

$$Q^2 + k\alpha_T (T_2 - T_1)Q + k\alpha_S S_0 F_1 = 0, \tag{14}$$

which gives two solutions. The one with the positive (negative) root is stable (unstable) and the bifurcation diagram of this model is shown in Fig. 5b for the case $T_2 < T_1$. When $F_1 < 0$ (freshwater input into the southern box), salt and temperature gradients work together to drive the AMOC. However, when $F_1 > 0$ freshwater input brakes the temperature driven AMOC and a saddle–node bifurcation occurs at $F_{1,c} = k\alpha_T^2 (T_2 - T_1)^2/(4\alpha_S S_0)$ with critical AMOC strength $Q_c = k\alpha_T (T_1 - T_2)/2$. What is important here is that the saddle–node bifurcation precisely occurs at the minimum of the AMOC induced southward freshwater transport $F_{ovS} = Q(S_2 - S_1)$ (the maximum of F_1) and that the multiple equilibrium regime (for $F_1 > 0$) is characterized by $F_{ovS} < 0$, i.e. the AMOC transports fresh water out of the Atlantic basin (into the southern box).

There are many variants of the inter-hemispheric Atlantic box models with focus on symmetry breaking [50,51] and studying the effect of atmospheric interactions [52,53]. All these conceptual models represent a very simplified view of the AMOC with limited spatial structure
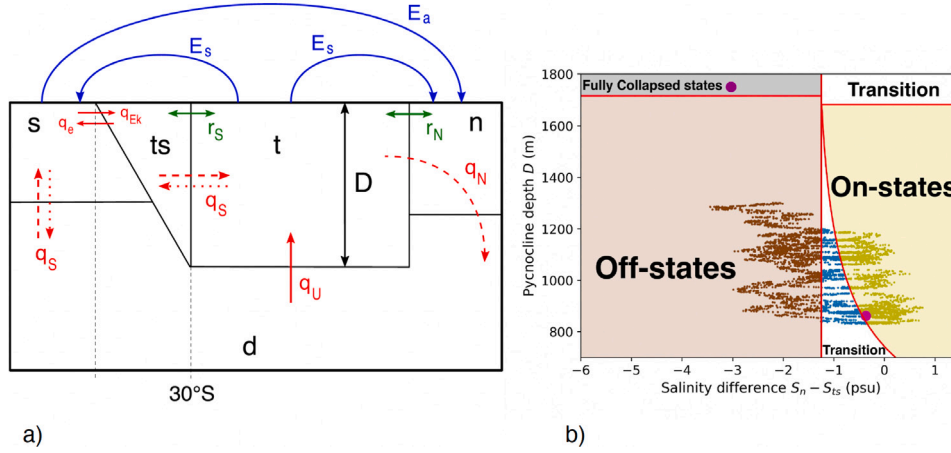
Fig. 6. (a) Sketch of the Cimatoribus et al. inter-hemispheric AMOC model [48], with a dynamic pycnocline depth D and salinity in five boxes as state vector. (b) An example of a long trajectory in the reduced phase space $(S_n - S_{ts}, D)$, for $(E_a, f_e) = (0.234, 0.4)$. The phase space contains 4 zones: on-states (yellow), off-states (brown), fully-collapsed states (grey) and a transition zone (white). The steady states are also indicated (purple dots). The red curves show the separation between each zone [49].

and only affected by advective and convective feedbacks due to the density–velocity field coupling. It was later realized that the AMOC is also determined by Southern Hemisphere winds [54], and is driven energetically by winds and tides [55]. A conceptual model that takes this additional physics schematically into account is the model by [56]. By combining it with the Stommel model, this model was extended by [57], and later on, by including an extra South-Atlantic box by [48,58]. This has led to more detailed conceptual inter-hemispheric Atlantic models of the AMOC of which the box geometry used in [58] is sketched in Fig. 6a.

Just to give an idea on the complexity of this model, the dimensional equations of this model for the salinities in the boxes and the pycnocline depth D are given by

$$\frac{d(V_t S_t)}{dt} = q_s(\mathcal{H}(q_s)S_{ts} + \mathcal{H}(-q_s)S_t) + q_u S_d$$
$$- \mathcal{H}(q_n)q_n S_t + r_s(S_{ts} - S_t) + r_n(S_n - S_t) + 2E_s S_0, \quad (15a)$$

$$\frac{d(V_{t_s} S_{ts})}{dt} = q_{Ek}S_s - q_e S_{ts} - q_s(\mathcal{H}(q_s)S_{ts} + \mathcal{H}(-q_s)S_t) + r_s(S_t - S_{ts}),$$
$$(15b)$$

$$\frac{d(V_n S_n)}{dt} = \mathcal{H}(q_n)q_n(S_t - S_n) + r_n(S_t - S_n) - (E_s + E_a)S_0, \quad (15c)$$

$$\frac{d(V_s S_s)}{dt} = q_s(\mathcal{H}(q_s)S_d + \mathcal{H}(-q_s)S_s) + q_e S_{ts} - q_{Ek}S_s - (E_s - E_a)S_0, \quad (15d)$$

$$(A + \frac{L_{x_A} L_y}{2})\frac{dD}{dt} = q_u + q_{Ek} - q_e - \mathcal{H}(q_n)q_n, \quad (15e)$$

$$S_0 V_0 = V_n S_n + V_d S_d + V_t S_t + V_{ts} S_{ts} + V_s S_s. \quad (15f)$$

where $\mathcal{H}$ is again the Heaviside function. The flows between the boxes are defined as:

$$q_{Ek} = \frac{\tau L_{xS}}{\rho_0 |f_S|} \; ; \; q_e = A_{GM}\frac{L_{xA}}{L_y}D \; ; \; q_s = q_{Ek} - q_e \; ;$$
$$q_n = \eta\frac{\rho_n - \rho_{ts}}{\rho_0}D^2 \; ; \; q_u = \frac{\kappa A}{D}, \quad (16)$$

where A is a cross section, the L's are all horizontal length scales, τ is a typical Southern Ocean zonal wind stress f_S is an average Coriolis parameter of the Southern Ocean, A_{GM} is an isopycnal mixing coefficient and η controls the density-AMOC relation. The terms with coefficients r_n and r_s represent wind driven transports. Again a linear equation of state is used and the volumes of the boxes t, ts and d are given by

$$V_t = AD \; ; \; V_{ts} = \frac{L_{xA}L_y}{D} \; ; \; V_d = V_0 - V_t - V_{ts} - V_n - V_s. \quad (17)$$

The freshwater forcing of the model is split into a symmetric component E_s and an asymmetric component E_a. For standard values

of the parameters, as given in [58], the bifurcation diagram of this model is again the back-to-back saddle node diagram. Further analysis shows that, in this case, and in accordance with the results in [47], the multiple equilibrium regime is characterized by an AMOC induced freshwater transport out of the Atlantic.

At least one attempt has been made to construct a model of the global meridional overturning circulation [59], and tune its parameters to model results from a low-resolution GCM, i.e. FAMOUS [60]. This global box model contains only salt balances and no representation of dynamical behavior of the pycnocline. The dynamics of this model was analyzed in detail in [61] and in addition to the back-to-back saddle–node bifurcations of the AMOC, they also find a subcritical Hopf bifurcation.

3.4. Stochastic conceptual AMOC models

From the deterministic models, it was learned that the AMOC can have a multiple equilibrium regime, and that this regime is characterized by an AMOC which transports freshwater out of the Atlantic basin. GCMs used in the Climate Model Intercomparison Project phase 6 (CMIP6) find that the AMOC strength will gradually decrease by the end of this century [62]. There are relatively little differences between the AMOC development under the various Shared Socioeconomic Pathways and no collapse occurs in these models. Of course, policy makers are interested in the probability of an AMOC collapse within a certain time period, say before the year 2100. What can conceptual models contribute to this issue?

With this question, two new aspects are introduced into conceptual models, e.g. the forcing is explicitly time dependent and the forcing contains a noisy component. Both aspects can be easily introduced into the model (4b). As $\alpha \gg 1$, we can approximate $x \sim 1$, and introducing white noise in the freshwater forcing plus an explicit time dependence gives the stochastic differential equation (SDE)

$$dY_t = (F_a(t) - Y_t(1 + \mu(1 - Y_t)^2))dt + \sigma dW_t, \quad (18)$$

where σ^2 measures the variance of the noise and W_t is the driving Wiener process.

Considering transient freshwater forcing in such models, three types of tipping behavior [9] can be distinguished (Fig. 7). In bifurcation-induced tipping the freshwater forcing is slowly increased, until it crosses a (saddle–node) bifurcation point (magenta dot). The system state tracks the strong AMOC branch, until it falls to the lower weak AMOC branch (Fig. 7a) due to an AMOC collapse. In rate-induced tipping, the rate of variation of the freshwater forcing is high, to the extent that the AMOC is no longer able to track the upper branch, and

Bifurcation tipping   **Rate-induced tipping**   **Noise-induced tipping**
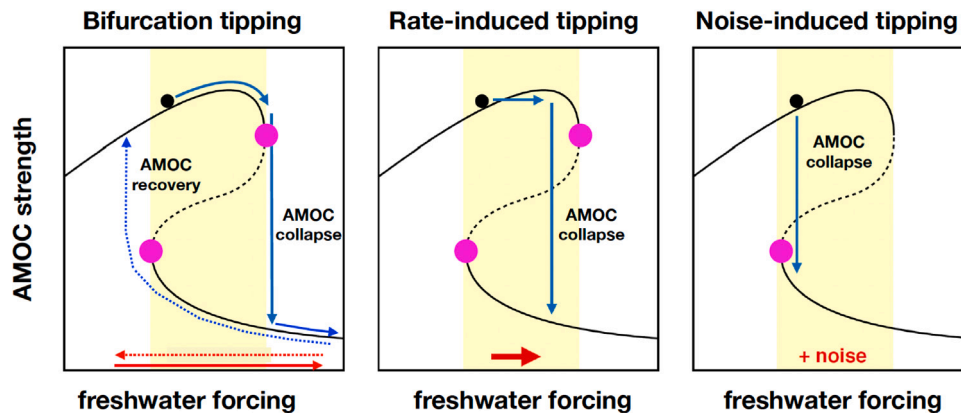
Fig. 7. Schematic of possible tipping behavior in a multi-stable (yellow region) stochastic model of the AMOC. Drawn (dotted) black curves: stable (unstable) steady states; black dot: initial state; magenta dot: saddle–node bifurcations; red arrow: freshwater forcing, where the thickness indicates the rate of change.

the system undergoes a transition to the lower branch (Fig. 7b). In noise-induced tipping [63], the freshwater forcing is kept constant, and small-scale processes (represented by noise) cause a transition from a strong to a weak AMOC (Fig. 7c). Rate-induced tipping has been studied in several conceptual AMOC models, for example in the Stommel two-box model coupled to a sea-ice model [64], and in a global box model [61]. Depending on the rate of the forcing, also overshoots may occur in AMOC transitions [65] and these have been studied using conceptual non-autonomous deterministic models in [66].

For the model (18) with a constant F_a, the transition probabilities from the strong AMOC state to the weak AMOC state (and vice-versa) were determined analytically using Kramer's formula in [31]. The effect of the type of noise (additive versus multiplicative) on the noise-induced transitions was studied in [67]. In [33], a periodic forcing component was included in the two-dimensional [31] model, i.e., $F(t) = \bar{F} + A \sin(2\pi t/T)$ and it was shown that stochastic resonance can occur. Here, a small periodic forcing and noise induce large transitions between the two stable equilibria of the AMOC. Stochastic conceptual AMOC models are reviewed in [68], with a focus on the effect of climate noise on decadal to centennial variability, on transitions between AMOC regimes and on their relevance to climate variability in the geological past.

In the model described by the Eqs. (15f) given above [58], the noise is prescribed in the asymmetric component of the freshwater flux E_a as

$$E_a = \bar{E}_a(1 + f_\sigma \zeta(t)), \tag{19}$$

where $\zeta(t)$ is a white noise process (zero mean and delta correlated). The transition probabilities were determined numerically versus the AMOC induced freshwater transport $F_{ovS} = -q_s(S_{ts} - S_d)$ and the freshwater noise amplitude f_σ. Determining transition probabilities using a naive Monte-Carlo simulation becomes quickly unfeasible when low probabilities of transitions are involved. For example, for a transition probability of 10^{-4}, already 10,000 simulations would be needed to likely simulate one event. Hence, several specialized methods have been developed to compute such transition probabilities more efficiently, such as Adaptive Multilevel Splitting [69] and Genealogical Particle Analysis [70]. Such methods are at the moment heavily used for the analysis of extremes in dynamical systems, specifically climate extremes [71].

In [58], the Trajectory Adaptive Multilevel Sampling (TAMS) method [72,73] was used and first estimates of AMOC transition probabilities were obtained [58]. In this model, two types of transitions were found: F-type transitions where the AMOC strength reduces but there is no full collapse ($q_n = 0, q_s > 0$), and S-type transitions where there is a full collapse ($q_n = 0, q_s < 0$). An example is shown in Fig. 6b where a long trajectory starting close to the steady on-state (strong AMOC state) is plotted. F-transitions can be seen through a transition

zone, but the time interval of the simulated trajectory is too short to undergo an S-transition.

The transition probabilities can be related to observable quantities, i.e., the amplitude of the freshwater noise and the indicator F_{ovS} (Fig. 8)). The red line in Fig. 8a shows this observed range and the most likely value (the black dot) indicates that there is a 15% probability that AMOC would collapse (in this model) within the next 100 years. The right panels illustrate the rapid increase of the transition probability with the noise amplitude f_σ, once this amplitude is large enough. Recently, there has been much effort to improve the TAMS algorithm using more efficient methods to compute the score function [49,74,75], with conceptual (AMOC) models as test cases.

3.5. AMOC tipping: mechanisms and interpretation

The usefulness of conceptual models can be evaluated on their capabilities of understanding mechanisms and providing an interpretation framework for results in models up in the hierarchy and eventually in observations. We will discuss this for the AMOC tipping, going through ocean-only models, EMICs and GCMs.

For relatively low-resolution 2D and 3D ocean-only models, bifurcation diagrams have been computed explicitly. The 2D (latitude-depth) THCM-Atlantic model (meridional resolution 4° with 16 vertical levels) has been used in the literature to investigate a multitude of problems associated with AMOC transitions [77,78]. The advantage of this model is that trajectories as well as full bifurcation diagrams (steady states and their stability) can be efficiently calculated. For the 3D (longitude–latitude-depth) THCM-Global model (resolution $3.75° \times 4.5°$ with 12 layers), explicit bifurcation diagrams have been computed with a surface freshwater flux anomaly γ_p (applied to a region in the northern North Atlantic, see inset in Fig. 9a) as parameter [76,79]. In this model, $\Sigma \sim F_{ovS}$ is indeed an excellent indicator for the AMOC multiple equilibrium regime [80]. Remember that when $F_{ovS} > 0$ ($F_{ovS} < 0$), the AMOC transports salt (freshwater) out of the Atlantic basin and there is a single (multiple) equilibrium regime (Fig. 9b).

When bifurcation diagrams cannot explicitly be computed, a (less precise) quantification of the multiple-equilibrium regime boundaries can be obtained by so-called quasi-equilibrium experiments. Here, the freshwater forcing is changed very slowly such that the model state stays close to the (slowly changing) equilibrium. When the freshwater forcing is varied in both directions and covers the multiple-equilibrium regime, regime boundaries can be inferred from the so-called hysteresis width, i.e. the freshwater forcing values where the AMOC collapses and recovers. The rate of forcing is important here and if much faster than the equilibration time scale of the steady state, the approximations of the regime boundaries become worse and also rate-induced tipping may occur [64]. An early result [81] with a low-resolution ocean-only
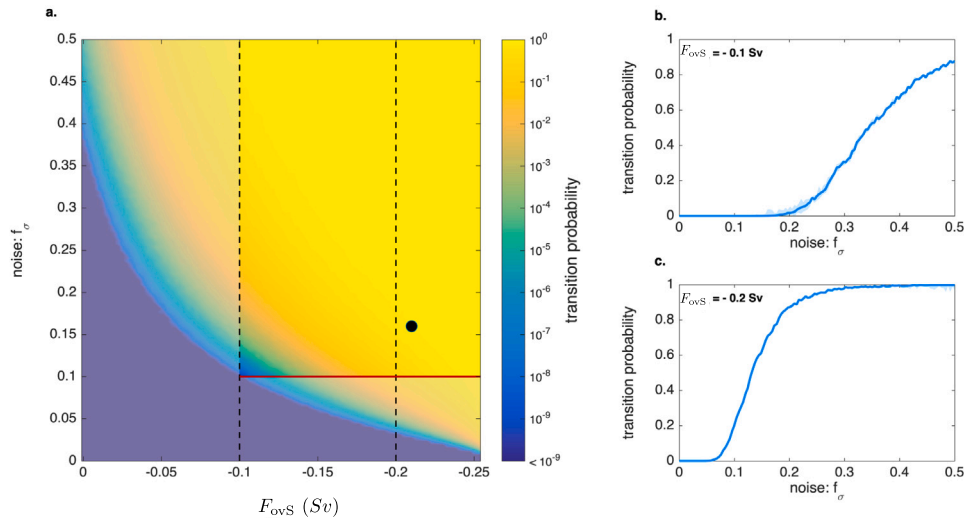
Fig. 8. (a) Results from [58] where probabilities for F-type AMOC transitions within 100 years were determined versus additive noise in freshwater forcing (f_σ) and the indicator F_{ovS}. The red box provides an estimate of the range of present-day F_{ovS} conditions. (b) Transition probabilities versus f_σ for $F_{ovS} = -0.1$ Sv. (c) Same as (b) but for $F_{ovS} = -0.2$ Sv.
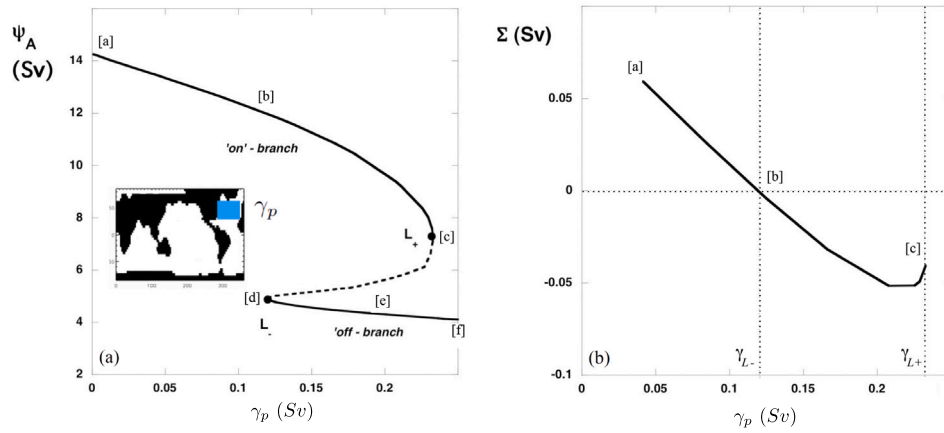
Fig. 9. (a) Bifurcation diagram under freshwater forcing γ_p (see inset) in the 3D THCM-Global model. Drawn (dashed) curves indicate stable (unstable) steady states. (b) Value of the stability indicator, here $\Sigma \sim F_{ovS}$, along the upper branch in (a).
Source: Figure from [76].
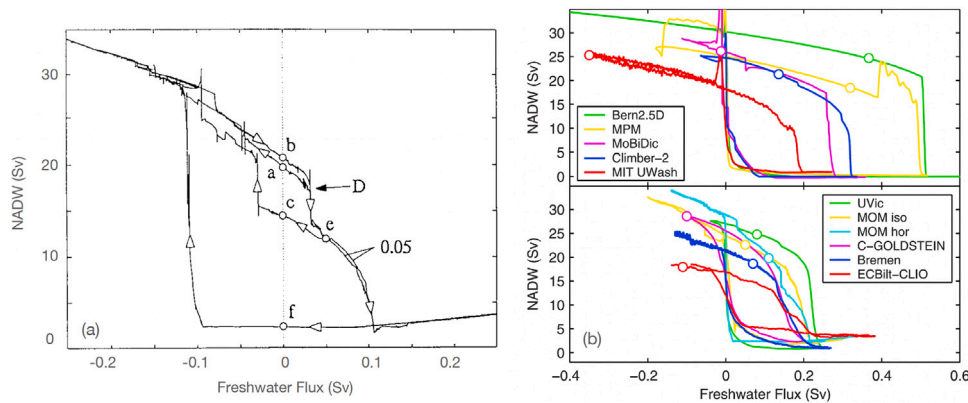
Fig. 10. (a) Trajectories computed with the global version of the MOM ([81], reprinted with permission of Springer Nature). On the vertical axis the amount of NADW (the AMOC strength) is plotted while on the horizontal axis, the strength of the freshwater forcing perturbation (in the northern North Atlantic) is plotted (in Sv). (b) Hysteresis diagrams based on quasi-equilibrium simulations of several EMICs ([82], reprinted with permission of John Wiley and Sons).

model (the Modular Ocean Model) is shown in Fig. 10a. There are clear indications of the saddle–node bifurcation structure, as found in conceptual models. Similar quasi-equilibrium experiments have also been performed with many EMICs [82] and relatively low-resolution global climate models such as the FAMOUS model [60]. In Fig. 10b, the response of the models is lined up when the AMOC recovers and the open circles indicate the unperturbed equilibrium state. There is wide range of hysteresis widths in these models, but they all indicate the existence of a multi-equilibrium regime.

However, there are also jumps to slightly different AMOC states in Fig. 10a. The interpretation of these jumps is that they are caused by convective transitions, as identified in the Welander model [39]. In a recent study [83], a more detailed bifurcation diagram was shown for the Python-based Veros model [84] based on many long simulations. Here, also a 'fragmented' bifurcation structure is found with many equilibria only differing in often grid-scale details. Rate-induced tipping was investigated in the same model [85], including sea-ice dynamics While it was thought that these convectively related jumps were spurious (i.e. not part of the governing equations) and due to numerical issues [77,86], recent work [87] on fragmented tipping had led to a different interpretation. An example problem studied in [87] is the PDE for the function $u(x, t)$, given by

$$\frac{\partial u}{\partial t} = \epsilon \frac{\partial^2 u}{\partial x^2} + u(1 - u^2) + \frac{1}{2} \cos \pi x + \mu, \tag{20}$$

where μ is the control parameter and $\epsilon \ll 1$. In this case, there is spatial inhomogeneity and small diffusion. Bifurcation diagrams including this spatial inhomogeneity show many additional saddle–node bifurcations leading to co-existing steady states [87]. Such a fragmentation of the bifurcation diagram indeed occurs in a typical Welander-type AMOC model (with but horizontal diffusion) of oceanic convection, as shown in [87].

In the FAMOUS model, it was shown that values of F_{ovS} are generally negative when there is overlap between strong and weak states of the AMOC. Also in the Community Climate System Model (CCSM3) AMOC hysteresis behavior has been found [88], but not with clear collapses or recoveries In state-of-the-art GCMs, due to computational constraints, in most cases only the AMOC response to particular freshwater forcing perturbations is considered. In these so-called 'hosing experiments' [89], quite a diversity of model behavior is found. It is not known yet whether a multiple-equilibrium AMOC regime exists in such models and only sporadic indications of such a regime have been found [90–92]. The problem is that it is difficult to assess whether the weak AMOC states computed are equilibrium solutions of the models because of the short integration time interval used [93,94]. Only very recently, a quasi-equilibrium simulation was performed with the Community Earth System Model (CESM) showing a wide hysteresis regime with a clear collapse and an even more spectacular recovery [95]. In the CESM, the collapse can be related to the minimum of F_{ovS} and the start of the recovery of the AMOC to the location where $F_{ovS} = 0$ on the AMOC on branch [96], in agreement with results of CCMs. The recovery is, however, strongly delayed by the presence of North Atlantic sea ice [95].

4. Summary and discussion

From the results described in the previous section, it is clear that CCMs have been important to generate the initial idea that tipping of the AMOC can occur [32,39] and that it is associated with bifurcation behavior in a nonlinear dynamical system giving rise to multiple equilibria. The existence of such multiple equilibria was subsequently found in many, more detailed models, such as 1D ocean-only models [97], 2D ocean-only models [51], 3D ocean-only models [98,99] and EMICs [82], the FAMOUS model [60] and most recently in the CESM [95]. The 'wrinkles' in these bifurcation diagrams, leading to additional saddle–node bifurcations and mostly in ocean-only models [83], are now interpreted as being due to fragmentation [87] and

caused by local convective feedback. The latter feedback was also identified first in CCMs [39,40].

A second important issue first identified in CCMs [99] is that the multiple equilibrium regime is characterized by the sign of the AMOC induced freshwater transport in/out of the Atlantic basin, indicated here by F_{ovS} [47]. The importance of this quantity has been demonstrated in 3D ocean-only models [80], EMICs [100], FAMOUS [60] and recently in CESM [95]. In all these models, the AMOC exports freshwater out of the Atlantic, under forcing conditions corresponding to a multiple equilibrium regime. The quantity F_{ovS} is observable [101,102] and its values indicate that the AMOC is in a multi-equilibrium regime. Sustained future section measurements (available since 2009) at 34°S from the SAMBA array [103,104] are therefore of utmost importance to reliable project future AMOC tipping [96].

Using CCMs, also first results on transition probabilities of noise-induced tipping under stationary, noisy forcing [58] were obtained. New computational techniques, such as TAMS, were used to determine transition probabilities and these are were applied already to a 2D AMOC model [78]. These are now being applied to models higher up in the hierarchy, such as 3D ocean-only models and EMICs [71]. However, algorithms such as TAMS need to be improved before they can be applied to more detailed models and there is a large effort at the moment in that direction [49]. With stochastic and transient forcing, techniques from statistical physics are also more and more applied to problems of AMOC dynamics. An overview is given in for studies of the climate system in general [3].

For the AMOC tipping example, the path from CCMs through the hierarchy to GCMs has been traversed and there is a reasonable consensus that mechanisms of tipping are understood within the full hierarchy of models. Along this path, a multitude of mathematical techniques has been applied to the CCMs, in particular bifurcation theory (both for autonomous and non-autonomous systems), ergodic theory and stochastic analysis [3,105,106]. The detailed mathematical analysis of some of the CCMs [41,87] has contributed importantly to the interpretation of the results in CCMs and GCMs. Also the more mathematical studies on the different types of tipping [9,41,65,87] have broadened the range of phenomena and also have helped to design numerical experiments in EMICs and GCMs. Researchers have put in much effort to analyze the GCM results, in terms of the concepts and observables developed in CCMs [91,92,107], which has helped enormously with bridging the results over the model hierarchy.

Of course, there remain many questions of the AMOC itself (e.g. what are its flow pathways, what determines the heat transport, how will it respond to climate change, what is its multi-decadal variability?), which remain to be figured out to a satisfying detail. This is currently done by a large observational effort in the OSNAP [38], RAPID [108] and SAMBA [103] programs, GCMs and also here CCMs can be very useful in the interpretation of the results [34,109]. All this work should help to address the earlier posed issue on the probability of an AMOC collapse before the year 2100. CMIP6 models probably are too stable for this task [93], likely due to biases in the freshwater forcing [110], and hence cannot provide a reliable answer to this problem yet.

The AMOC case serves as an example of how fruitful research in the area of Mathematics and Climate (and in general Mathematics of Planet Earth) can lead to scientific progress. A similar approach has, for example, also been successful in unraveling the mechanisms of ENSO. Leading conceptual models capturing the essential mechanisms are the recharge-oscillator model [111] and the delayed-oscillator model [112] and have been developed to better explain results of more detailed models [113]. In ENSO dynamics, equatorial wave propagation is crucial and hence differential delay equations (DDEs) arise naturally from the governing equations [112,114–116]. Conceptual models consisting of ODEs and DDEs have also been used to describe more detailed dynamics [117–121]. The connection between many CCM results and those in more detailed models is described in [79] (chapter 7) and [10] (chapter 8).

The climate research field offers many challenging problems for mathematicians, also in terms of the mathematics involved. Many of these problems are sometimes ignored for a long time by the climate research community, either because of a lack of expertise or because the detailed mathematical work is considered not rewarding enough. There are many areas in climate research where mathematicians are needed, such as stochastic partial differential equations, neural differential equations (or in general hybrid models) and computational techniques (such as rare event algorithms). Solving the more mathematical issues in collaboration with climate scientist can lead to a major step forward and to improved ESMs which are used for making more reliable climate projections.

Declaration of competing interest

The authors declare that they have no known competing financial interests or personal relationships that could have appeared to influence the work reported in this paper.

Data availability

No data was used for the research described in the article.

Acknowledgments

References

[1] H. Kaper, H. Engler, Mathematics and Climate, Society for Industrial and Applied Mathematics, Philadelphia, PA, 2013, http://dx.doi.org/10.1137/1.9781611972610, arXiv:https://epubs.siam.org/doi/pdf/10.1137/1.9781611972610. https://epubs.siam.org/doi/abs/10.1137/1.9781611972610.

[2] T.M. Lenton, J. Rockström, O. Gaffney, S. Rahmstorf, K. Richardson, W. Steffen, H.J. Schellnhuber, Climate tipping points — too risky to bet against, Nature 575 (7784) (2019) 592–595, http://dx.doi.org/10.1038/d41586-019-03595-0.

[3] M. Ghil, V. Lucarini, The physics of climate variability and climate change, Rev. Modern Phys. 92 (3) (2020) 035002, http://dx.doi.org/10.1103/revmodphys.92.035002, arXiv:1910.00583.

[4] M. Ghil, S. Childress, Topics in Geophysical Fluid Dynamics: Atmospheric Dynamics, Dynamo Theory, and Climate Dynamics, Springer-Verlag, Berlin/Heidelberg/New York, 1987.

[5] B. Saltzmann, Dynamical Paleoclimatology, Academic Press, 2001.

[6] H.A. Dijkstra, M. Ghil, Low-frequency variability of the large-scale ocean circulation: A dynamical systems approach, Rev. Geophys. 43 (3) (2005) 1–38.

[7] T.M. Lenton, H. Held, E. Kriegler, J.W. Hall, W. Lucht, S. Rahmstorf, H.J. Schellnhuber, Tipping elements in the Earth's climate system, Proc. Natl. Acad. Sci. USA 105 (6) (2008) 1786–1793, http://dx.doi.org/10.1073/pnas.0705414105, http://www.pubmedcentral.nih.gov/articlerender.fcgi?artid=2538841&tool=pmcentrez&rendertype=abstract.

[8] D.I. Armstrong McKay, A. Staal, J.F. Abrams, R. Winkelmann, B. Sakschewski, S. Loriani, I. Fetzer, S.E. Cornell, J. Rockström, T.M. Lenton, Exceeding 1.5 C global warming could trigger multiple climate tipping points, Science 377 (6611) (2022) eabn7950.

[9] P. Ashwin, S. Wieczorek, R. Vitolo, P. Cox, Tipping points in open systems: bifurcation, noise-induced and rate-dependent examples in the climate system, Phil. Trans. R. Soc. A 370 (2012) 1166–1184.

[10] H.A. Dijkstra, Nonlinear Climate Dynamics, Cambridge University Press, Cambridge, 2013.

[11] R.E. Zeebe, LOSCAR: Long-term ocean-atmosphere-sediment carbon cycle reservoir model v2.0.4, Geosci. Model Dev. 5 (1) (2012) 149–166, http://dx.doi.org/10.5194/gmd-5-149-2012.

[12] P. Kuma, F.A. Bender, A.R. Jönsson, Climate model code genealogy and its relation to climate feedbacks and sensitivity, J. Adv. Model. Earth Syst. 15 (7) http://dx.doi.org/10.1029/2022ms003588.

[13] IPCC, Climate change 2021: the physical science basis, in: Contribution of Working Group I to the Sixth Assessment Report of the Intergovernmental Panel on Climate Change, Climate Change Cambridge University Press, Cambridge, United Kingdom and New York, NY, USA, 2021, http://dx.doi.org/10.1017/9781009157896.

[14] M.e.a. Claussen, Earth system models of intermediate complexity: closing the gap in the spectrum of climate system models, Clim. Dynam. 18 (2002) 579–586.

[15] M. Willeit, A. Ganopolski, A. Robinson, N.R. Edwards, The Earth system model Climber-X v1.0, Part I: Climate model description and validation, Geosci. Model Dev. 15 (14) (2022) 5905–5948.

[16] P. Bakker, H. Goosse, D.M. Roche, Internal climate variability and spatial temperature correlations during the past 2000 years, Clim. Past 18 (11) (2022) 2523–2544, http://dx.doi.org/10.5194/cp-18-2523-2022, https://cp.copernicus.org/articles/18/2523/2022.

[17] M. Srokosz, M. Baringer, H. Bryden, S. Cunningham, T. Delworth, S. Lozier, J. Marotzke, R. Sutton, Past, present, and future changes in the atlantic meridional overturning circulation, Bull. Am. Meteorol. Soc. 93 (11) (2012) 1663–1676, http://dx.doi.org/10.1175/bams-d-11-00151.1.

[18] M.A. Srokosz, H.L. Bryden, Observing the Atlantic Meridional Overturning Circulation yields a decade of inevitable surprises, Science 348 (6241) (2015) 1255575, http://dx.doi.org/10.1126/science.1255575.

[19] M.W. Buckley, J. Marshall, Observations, inferences, and mechanisms of the Atlantic Meridional Overturning Circulation: A review, Rev. Geophys. 54 (1) (2016) 5–63, http://dx.doi.org/10.1002/2015rg000493.

[20] W. Johns, M. Baringer, L. Beal, Continuous, array-based estimates of Atlantic Ocean heat transport at 26.5 N, J. Clim. 24 (2011) 2429–2449.

[21] H.L. Bryden, H.R. Longworth, S.A. Cunnigham, Slowing down of the Atlantic meridional overturning circulation at 25°N, Nature 438 (2005) 655–657.

[22] E. Frajka-Williams, I.J. Ansorge, J. Baehr, H.L. Bryden, M.P. Chidichimo, S.A. Cunningham, G. Danabasoglu, S. Dong, K.A. Donohue, S. Elipot, P. Heimbach, N.P. Holliday, R. Hummels, L.C. Jackson, M. Karstensen, M. Lankhorst, I.A.L. Bras, M.S. Lozier, E.L. McDonagh, C.S. Meinen, H. Mercier, B.I. Moat, R.C. Perez, C.G. Piecuch, M. Rhein, M.A. Srokosz, K.E. Trenberth, S. Bacon, G. Forget, G. Goni, D. Kieke, J. Koelling, T. Lamont, G.D. McCarthy, C. Mertens, U. Send, D.A. Smeed, S. Speich, M. v. d. Berg, D. Volkov, C. Wilson, Atlantic meridional overturning circulation: Observed transport and variability, Front. Mar. Sci. 6 (2019) 1–18, http://dx.doi.org/10.3389/fmars.2019.00260.

[23] B.I. Moat, D.A. Smeed, E. Frajka-Williams, D.G. Desbruyères, C. Beaulieu, W.E. Johns, D. Rayner, A. Sanchez-Franks, M.O. Baringer, D. Volkov, L.C. Jackson, H.L. Bryden, Pending recovery in the strength of the meridional overturning circulation at 26°N, Ocean Sci. 16 (4) (2020) 863–874, http://dx.doi.org/10.5194/os-16-863-2020.

[24] L. Caesar, S. Rahmstorf, A. Robinson, G. Feulner, V. Saba, Observed fingerprint of a weakening Atlantic Ocean overturning circulation, Nature 556 (7700) (2018) 191–196, http://dx.doi.org/10.1038/s41586-018-0006-5.

[25] L. Caesar, G.D. McCarthy, D.J.R. Thornalley, N. Cahill, S. Rahmstorf, Current Atlantic Meridional Overturning Circulation weakest in last millennium, Nat. Geosci. 14 (3) (2021) 118–120, http://dx.doi.org/10.1038/s41561-021-00699-z.

[26] E.L. Worthington, B.I. Moat, D.A. Smeed, J.V. Mecking, R. Marsh, G.D. McCarthy, A 30-year reconstruction of the Atlantic meridional overturning circulation shows no decline, Ocean Sci. 17 (1) (2020) 285–299, http://dx.doi.org/10.5194/os-17-285-2021.

[27] J. Lynch-Stieglitz, The Atlantic meridional overturning circulation and abrupt climate change, Annu. Rev. Mar. Sci. 9 (1) (2016) 83–104, http://dx.doi.org/10.1146/annurev-marine-010816-060415.

[28] L.G. Henry, J.F. McManus, W.B. Curry, N.L. Roberts, A.M. Piotrowski, L.D. Keigwin, North Atlantic ocean circulation and abrupt climate change during the last glaciation, Science 353 (6298) (2016) 470–474, http://dx.doi.org/10.1126/science.aaf5529.

[29] W. Dansgaard, Evidence for general instability of past climate from a 250-kyr ice-core record, Nature 364 (1993) 218–220.

[30] S. Rahmstorf, Ocean circulation and climate changes during the past 120, 000 years, Nature 419 (2002) 207–214.

[31] P. Cessi, A simple box model of stochastically forced thermohaline flow, J. Phys. Oceanogr. 24 (1994) 1911–1920.

[32] H. Stommel, Thermohaline convection with two stable regimes of flow, Tellus 2 (1961) 244–230.

[33] P. Velez-Belchi, A. Alvarez, P. Colet, J. Tintore, R.L. Haney, Stochastic resonance in the thermohaline circulation, Geophys. Res. Lett. 28 (2001) 2053–2056.

[34] J. Marotzke, Abrupt climate change and thermohaline circulation: Mechanisms and Predictability, Proc. Natl. Acad. Sci. 97 (2000) 1347–1350.

[35] Y.G. Park, The stability of thermohaline circulation in a two-box model, J. Phys. Oceanogr. 29 (1999) 3101–3110.

[36] E. Tziperman, L. Stone, M.A. Cane, H. Jarosh, El Niño chaos: overlapping of resonances between the seasonal cycle and the Pacific ocean-atmosphere oscillator, Science 264 (1994) 72–74.

[37] A. Neff, A. Keane, H.A. Dijkstra, B. Krauskopf, Bifurcation Analysis of a North Atlantic Ocean Box Model with Two Deep-Water Formation Sites, 2023, pp. 1–21, http://dx.doi.org/10.48550/arXiv.2305.11975.

[38] M.S. Lozier, F. Li, S. Bacon, F. Bahr, A.S. Bower, S.A. Cunningham, M.F. d. Jong, L. d. Steur, B. deYoung, J. Fischer, S.F. Gary, B.J.W. Greenan, N.P. Holliday, A. Houk, L. Houpert, M.E. Inall, W.E. Johns, H.L. Johnson, C. Johnson, J. Karstensen, G. Koman, I.A.L. Bras, X. Lin, N. Mackay, D.P. Marshall, H. Mercier, M. Oltmanns, R.S. Pickart, A.L. Ramsey, D. Rayner, F. Straneo, V. Thierry, D.J. Torres, R.G. Williams, C. Wilson, J. Yang, I. Yashayaev, J. Zhao, A sea change in our view of overturning in the subpolar North Atlantic, Science 363 (6426) (2019) 516–521, http://dx.doi.org/10.1126/science.aau6592.

[39] P. Welander, A simple heat-salt oscillator, Dyn. Atmos. Oceans 6 (1982) 233–242.

[40] P. Cessi, Convective adjustment and thermohaline excitability, J. Phys. Oceanogr. 26 (1996) 481–491.

[41] J. Bailie, B. Krauskopf, Bifurcation analysis of a conceptual model for the Atlantic Meridional Overturning Circulation, 2023, pp. 1–35, http://dx.doi.org/10.48550/arXiv.2307.16414.

[42] A. Colin de Verdière, A simple model of millennial oscillations of the thermohaline circulation, J. Phys. Oceanogr. 37 (5) (2007) 1142–1155.

[43] A. Colin de Verdière, The instability of the thermohaline circulation in a low-order model, J. Phys. Oceanogr. 40 (2010) 757–773.

[44] M. Winton, E.S. Sarachik, Thermohaline oscillations induced by strong steady salinity forcing of ocean general circulation models, J. Phys. Oceanogr. 23 (1993) 1389–1410.

[45] H. Gildor, E. Tziperman, Sea ice as the glacial cycles climate switch: Role of seasonal and orbital forcing, Paleoceanography 15 (2000) 605–615.

[46] C. Rooth, Hydrology and ocean circulation, Prog. Oceanogr. 11 (1982) 131–149.

[47] S. Rahmstorf, On the freshwater forcing and transport of the Atlantic thermo-haline circulation, Clim. Dynam. 12 (12) (1996) 799–811, http://dx.doi.org/10.1007/s003820050144.

[48] A. Cimatoribus, S. Drijfhout, M. Toom, H. Dijkstra, Sensitivity of the Atlantic meridional overturning circulation to South Atlantic freshwater anomalies, Clim. Dynam. 39 (2012) 2291–2306, http://dx.doi.org/10.1007/s00382-012-1292-5.

[49] V. Jacques-Dumas, R.M.v. Westen, F. Bouchet, H.A. Dijkstra, Data-driven meth-ods to estimate the committor function in conceptual ocean models, Nonlinear Processes Geophys. 30 (2) (2023) 195–216, http://dx.doi.org/10.5194/npg-30-195-2023, arXiv:2306.17049.

[50] P. Welander, Thermohaline effects in the ocean circulation and related sim-ple models, in: J. Willebrand, D.L.T. Anderson (Eds.), Large-Scale Transport Processes in Oceans and Atmosphere, D. Reidel, 1986, pp. 163–200.

[51] O. Thual, J.C. McWilliams, The catastrophe structure of thermohaline convec-tion in a two-dimensional fluid model and a comparison with low-order box models, Geophys. Astrophys. Fluid Dyn. 64 (1992) 67–95.

[52] V. Lucarini, P.H. Stone, Thermohaline circulation stability: A box model study. Part I: Uncoupled model, J. Clim. 18 (4) (2005) 501–513, http://dx.doi.org/10.1175/JCLI-3278.1, https://journals.ametsoc.org/view/journals/clim/18/4/jcli-3278.1.xml.

[53] V. Lucarini, P.H. Stone, Thermohaline circulation stability: A box model study. Part II: Coupled atmosphere–ocean model, J. Clim. 18 (4) (2005) 514–529, http://www.jstor.org/stable/26253408.

[54] J.R. Toggweiler, B. Samuels, On the ocean's large scale circulation in the limit of no vertical mixing, J. Phys. Oceanogr. 28 (1998) 1832–1852.

[55] W. Munk, C. Wunsch, Abyssal recipes II: energetics of tidal and wind mixing, Deep-Sea Res. 45 (1998) 1977–2010.

[56] A. Gnanadesikan, A simple predictive model of the structure of the oceanic pycnocline, Science 283 (1999) 2077–2081.

[57] H.L. Johnson, D.P. Marshall, D.A.J. Sproson, Reconciling theories of a mechan-ically driven meridional overturning circulation with thermohaline forcing and multiple equilibria, Clim. Dynam. 29 (7–8) (2007) 821–836, http://dx.doi.org/10.1007/s00382-007-0262-9.

[58] D. Castellana, S. Baars, F.W. Wubs, H.A. Dijkstra, Transition probabilities of noise-induced transitions of the atlantic ocean circulation, Sci. Rep. 9 (1) (2019) 1–7.

[59] R.A. Wood, J.M. Rodríguez, R.S. Smith, L.C. Jackson, E. Hawkins, Observ-able, low-order dynamical controls on thresholds of the atlantic meridional overturning circulation, Clim. Dynam. 53 (2019) 6815–6834.

[60] E. Hawkins, R.S. Smith, L.C. Allison, J.M. Gregory, T.J. Woollings, H. Pohlmann, B. De Cuevas, Bistability of the Atlantic overturning circulation in a global climate model and links to ocean freshwater transport, Geophys. Res. Lett. 38 (10) (2011) L10605.

[61] H. Alkhayuon, P. Ashwin, L.C. Jackson, C. Quinn, R.A. Wood, Basin bifurca-tions, oscillatory instability and rate-induced thresholds for AMOC in a global oceanic box model, Proc. R. Soc. 475 (2019) 20190051, http://dx.doi.org/10.1098/rspa.2019.0051.

[62] W. Weijer, W. Cheng, O.A. Garuba, A. Hu, B.T. Nadiga, CMIP6 models predict significant 21st century decline of the Atlantic meridional overturning circulation, Geophys. Res. Lett. 47 (12) (2020) e2019GL08607, http://dx.doi.org/10.1029/2019gl086075.

[63] P.D. Ditlevsen, S.J. Johnsen, Tipping points: Early warning and wishful thinking, Geophys. Res. Lett. 37 (19) (2010) L19703.

[64] J. Lohmann, D. Castellana, P.D. Ditlevsen, H.A. Dijkstra, Abrupt climate change as rate-dependent cascading tipping point, Earth Syst. Dyn. 2021 (2021) 1–25, http://dx.doi.org/10.5194/esd-2021-7, https://esd.copernicus.org/preprints/esd-2021-7/.

[65] C. Kuehn, A mathematical framework for critical transitions: Bifurcations, fast–slow systems and stochastic dynamics, Physica D 240 (12) (2011) 1020–1035.

[66] P.D.L. Ritchie, J.J. Clarke, P.M. Cox, C. Huntingford, Overshooting tipping point thresholds in a changing climate, Nature 592 (7855) (2021) 517–523, http://dx.doi.org/10.1038/s41586-021-03263-2.

[67] A. Timmermann, G. Lohmann, Noise-induced transitions in a simplified model of the thermohaline circulation, J. Phys. Oceanogr. 30 (2000) 1891–1900.

[68] A.H. Monahan, J. Alexander, A.J. Weaver, Stochastic models of the meridional overturning circulation: time scales and patterns of variability, Phil. Trans. R. Soc. A 366 (1875) (2008) 2525–2542, http://dx.doi.org/10.1098/rsta.2008.0045.

[69] J. Rolland, E. Simonnet, Statistical behaviour of adaptive multilevel splitting algorithms in simple models, J. Comput. Phys. 283 (C) (2015) 541–558, http://dx.doi.org/10.1016/j.jcp.2014.12.009.

[70] J. Wouters, F. Bouchet, Rare event computation in deterministic chaotic systems using genealogical particle analysis, J. Phys. A 49 (37) (2016) 374002, http://dx.doi.org/10.1088/1751-8113/49/37/374002.

[71] F. Ragone, F. Bouchet, Rare event algorithm study of extreme warm summers and heatwaves over Europe, Geophys. Res. Lett. 48 (12) http://dx.doi.org/10.1029/2020gl091197, arXiv:2009.02519.

[72] T. Lestang, F. Ragone, C.-E. Bréhier, C. Herbert, F. Bouchet, Computing return times or return periods with rare event algorithms, J. Stat. Mech. Theory Exp. 2018 (4) (2018) 043213.

[73] E. Simonnet, J. Rolland, F. Bouchet, Multistability and rare spontaneous transitions in barotropic β-plane turbulence, J. Atmosph. Sci. 78.

[74] D. Lucente, S. Duffner, C. Herbert, J. Rolland, F. Bouchet, Machine learning of committor functions for predicting high impact climate events. arXiv, eprint: 1910.11736. arXiv:1910.11736.

[75] P. Wang, D. Castellana, H.A. Dijkstra, Improvements to the use of the Trajectory-Adaptive Multilevel Sampling algorithm for the study of rare events, Nonlinear Processes Geophys. 28 (1) (2021) 135–151, http://dx.doi.org/10.5194/npg-28-135-2021.

[76] S.E. Huisman, M. den Toom, H.A. Dijkstra, S. Drijfhout, An indicator of the multiple equilibria regime of the atlantic meridional overturning circulation, J. Phys. Oceanogr. 40 (3) (2010) 551–567.

[77] M. Den Toom, H.A. Dijkstra, F.W. Wubs, Spurious multiple equilibria introduced by convective adjustment, Ocean Model. 38 (1–2) (2011) 126–137.

[78] S. Baars, D. Castellana, F. Wubs, H. Dijkstra, Application of adaptive multilevel splitting to high-dimensional dynamical systems, J. Comput. Phys. 424 (2021) 109876, http://dx.doi.org/10.1016/j.jcp.2020.109876, arXiv:2011.05745.

[79] H.A. Dijkstra, W. Weijer, Stability of the global ocean circulation: basic bifurcation diagrams, J. Phys. Oceanogr. 35 (2005) 933–948.

[80] H.A. Dijkstra, Characterization of the multiple equilibria regime in a global ocean model, Tellus (2007) 695–705.

[81] S. Rahmstorf, Multiple convection patterns and thermohaline flow in an idealized OGCM, J. Clim. 8 (1995) 3028–3039.

[82] S. Rahmstorf, M. Crucifix, A. Ganopolski, H. Goosse, I. Kamenkovich, R. Knutti, G. Lohmann, R. Marsh, L.A. Mysak, Z. Wang, A.J. Weaver, Thermohaline circulation hysteresis: A model intercomparison, Geophysical Research Letters 32 (2005) L23605, http://dx.doi.org/10.1029/2005GL023655.

[83] J. Lohmann, H.A. Dijkstra, M. Jochum, V. Lucarini, P.D. Ditlevsen, Multistability and Intermediate tipping of the Atlantic Ocean Circulation, 2023, pp. 1–26, http://dx.doi.org/10.48550/arXiv.2304.05664.

[84] D. Häfner, R.L. Jacobsen, C. Eden, M.R.B. Kristensen, M. Jochum, R. Nuterman, B. Vinter, Veros v0.1 – a fast and versatile ocean simulator in pure Python, Geosci. Model Dev. 11 (8) (2018) 3299–3312, http://dx.doi.org/10.5194/gmd-11-3299-2018, https://gmd.copernicus.org/articles/11/3299/2018/.

[85] J. Lohmann, P.D. Ditlevsen, Risk of tipping the overturning circulation due to increasing rates of ice melt, Proc. Natl. Acad. Sci. 118 (9) (2021) e2017989118, http://dx.doi.org/10.1073/pnas.2017989118.

[86] M. Vellinga, Multiple equilibria of the thermohaline circulation as a side effect of convective adjustment, J. Phys. Oceanogr. 28 (1998) 305–319.

[87] R. Bastiaansen, H.A. Dijkstra, A.S. von der Heydt, Fragmented tipping in a spatially heterogeneous world, Environ. Res. Lett. 17 (4) (2022) 045006, http://dx.doi.org/10.1088/1748-9326/ac59a8.

[88] A. Hu, G.A. Meehl, W. Han, A. Timmermann, B. Otto-Bliesner, Z. Liu, W.M. Washington, W. Large, A. Abe-Ouchi, M. Kimoto, K. Lambeck, B. Wu, Role of the Bering Strait on the hysteresis of the ocean conveyor belt circulation and glacial climate stability, Proc. Natl. Acad. Sci. 109 (17) (2012) 6417–6422, http://dx.doi.org/10.1073/pnas.1116014109.

[89] R.J. Stouffer, J. Yin, J.M. Gregory, K.W. Dixon, M.J. Spelman, W. Hurlin, A.J. Weaver, M. Eby, G.M. Flato, H. Hasumi, A. Hu, J.H. Jungclaus, I.V. Kamenkovich, A. Levermann, M. Montoya, S. Murakami, S. Nawrath, A. Oka, W.R. Peltier, D.Y. Robitaille, A.P. Sokolov, G. Vettoretti, S.L. Weber, Investigating the causes of the response of the thermohaline circulation to past and future climate changes, J. Clim. 19 (2006) 1365–1387.

[90] J.V. Mecking, S.S. Drijfhout, L.C. Jackson, T. Graham, Stable AMOC off state in an eddy-permitting coupled climate model, Clim. Dynam. 47 (7) (2016) 2455–2470, http://dx.doi.org/10.1007/s00382-016-2975-0.

[91] L.C. Jackson, R.A. Wood, Timescales of AMOC decline in response to fresh water forcing, Clim. Dynam. 51 (4) (2018) 1333–1350, http://dx.doi.org/10.1007/s00382-017-3957-6.

[92] L.C. Jackson, R.A. Wood, Hysteresis and resilience of the AMOC in an eddy-permitting GCM, Geophys. Res. Lett. 45 (16) (2018) 8547–8556, http://dx.doi.org/10.1029/2018gl078104.

[93] W. Weijer, W. Cheng, S.S. Drijfhout, A.V. Fedorov, A. Hu, L.C. Jackson, W. Liu, E.L. McDonagh, J.V. Mecking, J. Zhang, Stability of the atlantic meridional overturning circulation: A review and synthesis, J. Geophys. Res.-Oceans 124 (8) (2019) 5336–5375, http://dx.doi.org/10.1029/2019jc015083.

[94] L.C. Jackson, A. Biastoch, M.W. Buckley, D.G. Desbruyères, E. Frajka-Williams, B. Moat, J. Robson, The evolution of the North Atlantic meridional overturning circulation since 1980, Nat. Rev. Earth Environ. 3 (4) (2022) 241–254.

[95] R.M. van Westen, H.A. Dijkstra, Asymmetry of AMOC Hysteresis in a State-of-the-Art Global Climate Model, 2023, pp. 1–29, http://dx.doi.org/10.48550/arXiv.2308.14098.

[96] R.M. van Westen, M. Kliphuis, H.A. Dijkstra, New Physics-Based Early Warning Signal shows AMOC is on Tipping Course, 2023, pp. 1–29, http://dx.doi.org/10.48550/arXiv.2308.01688.

[97] P. Cessi, W.R. Young, Multiple equilibria in two-dimensional thermohaline circulation, J. Fluid Mech. 241 (1992) 291–309.

[98] F.O. Bryan, High-latitude salinity effects and interhemispheric thermohaline circulations, Nature 323 (1986) 301–304.

[99] S. Rahmstorf, J. Marotzke, J. Willebrand, Stability of the thermohaline circulation, in: W.A. Kraus (Ed.), The Warmwatersphere of the North Atlantic Ocean, Borntraeger, Berlin-Stuttgart, Germany, 1996, pp. 129–158.

[100] P. de Vries, S.L. Weber, The Atlantic freshwater budget as a diagnostic for the existence of a stable shut down of the meridional overturning circulation, Geophys. Res. Lett. 32 (9) (2005) L09606.

[101] H.L. Bryden, B.A. King, G.D. McCarthy, South Atlantic overturning circulation at 24S, J. Mar. Res. 69 (2011) 38–55.

[102] S.L. Garzoli, M.O. Baringer, S. Dong, R.C. Perez, Q. Yao, South Atlantic meridional fluxes, Deep Sea Res. I: Oceanogr. Res. Pap. 71 (2013) 21–32.

[103] C.S. Meinen, S. Speich, A.R. Piola, I. Ansorge, E. Campos, M. Kersalé, T. Terre, M.P. Chidichimo, T. Lamont, O.T. Sato, et al., Meridional overturning circulation transport variability at 34.5S during 2009–2017: Baroclinic and barotropic flows and the dueling influence of the boundaries, Geophys. Res. Lett. 45 (9) (2018) 4180–4188.

[104] M. Kersalé, C.S. Meinen, R.C. Perez, A.R. Piola, S. Speich, E.J.D. Campos, S.L. Garzoli, I. Ansorge, D.L. Volkov, M.L. Hénaff, S. Dong, T. Lamont, O.T. Sato, M.v.d. Berg, Multi-year estimates of daily heat transport by the Atlantic meridional overturning circulation at 34.5°S, J. Geophys. Res.: Oceans 126 (5) http://dx.doi.org/10.1029/2020jc016947.

[105] M. Ghil, M. Chekroun, E. Simonnet, Climate dynamics and fluid mechanics: Natural variability and related uncertainties, Physica D 237 (14–17) (2008) 2111–2126.

[106] M.D. Chekroun, E. Simonnet, M. Ghil, Stochastic climate dynamics: Random attractors and time-dependent invariant measures, Physica D 240 (21) (2011) 1685–1700.

[107] J.V. Mecking, S.S. Drijfhout, L.C. Jackson, M.B. Andrews, The effect of model bias on Atlantic freshwater transport and implications for AMOC bi-stability, Tellus Ser. A-Dyn. Meteorol. Oceanogr. (2017) 1–15, http://dx.doi.org/10.1080/16000870.2017.1299910.

[108] S. Cunningham, T. Kanzow, D. Rayner, M. Baringer, W. Johns, J. Marotzke, H. Longworth, E. Grant, J. Hirschi, L. Beal, et al., Temporal Variability of the Atlantic Meridional Overturning Circulation at 26.5° N, Science 317 (5840) (2007) 935.

[109] J. Marotzke, Boundary mixing and the dynamics of three-dimensional thermohaline circulations, J. Phys. Oceanogr. 27 (8) (1997) 1713–1728.

[110] R.M. van Westen, H.A. Dijkstra, Persistent climate model biases in the Atlantic ocean's freshwater transport, EGUsphere (2023) 1–29, http://dx.doi.org/10.5194/egusphere-2023-1502.

[111] F.-F. Jin, An equatorial recharge paradigm for ENSO. I: Conceptual Model, J. Atmos. Sci. 54 (1997) 811–829.

[112] M. Suarez, P. Schopf, A delayed action oscillator for ENSO, J. Atmos. Sci. 45 (21) (1988) 3283–3287.

[113] S. Zebiak, M. Cane, A model of El Nino-Southern Oscillation, Mon. Weather Rev. 115 (31) http://academiccommons.columbia.edu/catalog/ac%3A145611.

[114] F.-F. Jin, An equatorial recharge paradigm for ENSO. II: A stripped-down coupled model, J. Atmos. Sci. 54 (1997) 830–8847.

[115] A. Keane, B. Krauskopf, C.M. Postlethwaite, Climate models with delay differential equations, Chaos 27 (11) (2017) 114309–114316, http://dx.doi.org/10.1063/1.5006923.

[116] S.K.J. Falkena, C. Quinn, J. Sieber, J. Frank, H.A. Dijkstra, Derivation of delay equation climate models using the Mori-Zwanzig formalism, Proc. R. Soc. A Math. Phys. Eng. Sci. 475 (2227) (2019) 20190075, http://dx.doi.org/10.1098/rspa.2019.0075.

[117] A. Timmermann, F.F. Jin, J. Abshagen, A nonlinear theory of El Niño bursting, J. Atmosph. Sci. 60 (2003) 165–176.

[118] A. Keane, B. Krauskopf, H.A. Dijkstra, The effect of state dependence in a delay differential equation model for the El Niño Southern Oscillation, Philos. Trans. R. Soc. A-Math. Phys. Eng. Sci. 377 (2153) (2019) 20180121–20180123, http://dx.doi.org/10.1098/rsta.2018.0121, https://royalsocietypublishing.org/doi/pdf/10.1098/rsta.2018.0121.

[119] A. Roberts, J. Guckenheimer, E. Widiasih, A. Timmermann, C.K.R.T. Jones, Mixed-mode oscillations of El Niño–Southern oscillation, J. Atmos. Sci. 73 (4) (2016) 1755–1766, http://dx.doi.org/10.1175/JAS-D-15-0191.1.

[120] M. Chekroun, J. Neelin, D. Kondrashov, J. McWilliams, M. Ghil, Rough parameter dependence in climate models and the role of ruelle-pollicott resonances, Proc. Natl. Acad. Sci. USA 111 (5) (2014) 1684–1690.

[121] J. Guckenheimer, A. Timmermann, H. Dijkstra, A. Roberts, (Un)predictability of strong El Niño events, Dyn. Stat. Clim. Syst. 2 (1) (2017) 2399–2412.